Polymer Degradation and Stability 184 (2021) 109476

Contents lists available at ScienceDirect

Polymer Degradation and Stability

journal homepage: www.elsevier.com/locate/polymdegradstab

Accelerated Photodegradation of Solid Phase Polystyrene by Nano TiO_2-Graphene Oxide Composite under Ultraviolet radiation

Dinoop lal S[a], Sunil Jose T[a,*], Rajesh C[b], Arun KJ[c]

[a] Dept. of Chemistry, St.Thomas' College, Thrissur, Kerala, India, 680 001
[b] Dept of Chemistry, MES Keveeyam College, Valanchery, Malappuram, Kerala, India, 676552
[c] Department of Physics, Sree Kerala Varma College, Thrissur, Kerala, India, 680011

ARTICLE INFO

Article history:
Received 16 January 2020
Revised 25 September 2020
Accepted 29 December 2020
Available online 31 December 2020

Keywords:
Nano TiO_2-GO composite
Hydrothermal method
Polystyrene
UV radiation
photodegradation
Chain scission

ABSTRACT

Nano TiO_2-graphene oxide (TiO_2-GO) composites with varying weight percentages of GO were successfully developed by ultrasonication assisted hydrothermal approach and characterised. HRTEM analysis revealed that the GO sheets associated with TiO_2 have broken down into nano dimensions. Photodegradation of polystyrene (PS), PS-TiO_2 and PS-TiO_2-GO composites were studied under UV irradiation of wavelength 253 nm. Nano TiO_2-GO loaded solid phase polystyrene (PS) underwent an accelerated photodegradation compared to Pristine PS and PS-TiO_2 composite as evident from various monitoring techniques. Gel permeation chromatography (GPC) revealed that the degradation proceeded through random chain scissions decreasing the average molecular weights. PS and PS composites followed the mechanism of photo oxidative degradation as evident from FTIR. Maximum degradation percentage was observed in PS-TiO_2-30%GO compared to the other specimens under study. Mechanical properties including tensile and flexural strengths which were found to be higher for the PS composites compared to pristine PS, decreased appreciably upon UV irradiation due to deterioration of polymer chain. Dielectric strength of the PS composites also decreased as a consequence of photodegradation revealing the formation of charge centers within the polymer chain. Dielectric permittivity of the polymer specimens under study increased upon UV irradiation suggesting the formation of more polar centers. The improved thermal stability of PS composites compared to pristine PS decreased due to photodegradation of the polymer chain. The glass transition temperature (Tg) and decomposition temperature lowered as a consequence of chain scission of polymer specimens caused by photodegradation. Photocatalytic activity of nano TiO_2 was enhanced upon its surface modification using GO for the photodegradation of PS under UV radiation.

1. Introduction

Increased consumption of plastic commodities worldwide has led to a steep rise in the total amount of plastic debris. The uncontrollable spread of plastic wastes which have adverse effects on the environment has become one of the primary concerns of most of the countries. Only a very few percentage of plastic debris are being recycled or incinerated. Incineration of plastics further produces several hazardous secondary side products [1]. Most of plastic debris ends up in land filling. The objective of our work is to demolish such plastic debris without much environmental issues.

Polystyrene (PS) - one of the most widely used plastic was chosen for our investigation. PS undergoes degradation when exposed to sunlight [2]. The process – termed as photodegradation deteriorates the polymer rendering it as a useless material with degraded properties. Chain scission, mass loss, brittleness etc. are consequences of photodegradation [3,4]. The process of photodegradation is however quiet slow and depends upon the intensity of UV radiation to which the plastic is exposed. Studies have shown that the rate of photodegradation could be enhanced by the aid of various photocatalysts loaded into the PS matrix [5].

Transition metal oxide semiconductors exhibit appreciable photocatalytic activity for the degradation of PS. Nano TiO_2 (anatase phase) was found to be the best out of other metal oxide photocatalysts due to its high efficiency, nontoxicity, photostability, cheapness, reusability and easy synthetic approach. TiO_2 absorbs UV radiations from the sunlight as its optical band gap energy range between 3.2-3.5 eV (depending upon the particle size) [6]. Electron- hole pair generated upon interaction of TiO_2 with UV light further interacts with adsorbed oxygen, water and hydroxyl groups (-OH) to produce various active species which are trans-

* Corresponding author. Dr. Sunil Jose T, Assistant professor, Department of Chemistry, St. Thomas' College (Affiliated to University of Calicut), Thrissur, Kerala, India. 680 001.
E-mail address: sjtppc@gmail.com (S.J. T).

https://doi.org/10.1016/j.polymdegradstab.2020.109476
0141-3910/

ferred into PS matrix leading to radical initiated photodegradation reactions. The efficiency of TiO_2 could not be totally utilized due to instantaneous recombination of electron- hole pairs after their formation [7]. Studies to minimize the electron- hole combination have been done worldwide and appreciable results were achieved. Some of these techniques included doping TiO_2 with metals [8–10], coupling TiO_2 with other metal chalcogens [11,12], organometallic compounds [13], organic photosensitizers [14], incorporation of TiO_2 with carbon compounds (CNTs, fullerenes, graphene etc) and so on [15]. Water purification studies implement the application of electron, hole and -OH radical scavengers which reduces the possibility of electron hole recombination [16].

In this piece of work we have chosen graphene oxide (GO) incorporated TiO_2 for accelerated photocatalytic degradation of PS. GO could be considered as a derivative of graphene with oxygen atoms bonded covalently to some of its carbon atoms leading to hydroxyl or epoxy bonds. Carboxylic acid functional groups may also be attached to the periphery of the hexagonal two dimensional planes of GO [17]. Graphene is a well celebrated material with wide varieties of application and scope due its p-electron configuration similar to benzene ring along its 2D planar network. Its unique properties include enhanced electrical [18], mechanical [19], thermal [20] and optical properties [21]. Enhanced chemical stability is also observed [22]. In our work, we considered GO instead of graphene as the surface modifier of nano TiO_2 keeping in mind the following aspects: (i) GO bears similar properties as graphene. (ii) GO could stabilize nano TiO_2 much easier than graphene by hydrogen bond. (iii) The oxygen containing functional groups present in GO can interact with electrons from TiO_2 forming a bridge between them. (iv) The functional groups present in GO could produce radicals when exposed to UV radiation for the initiation of photochemical reaction. (v) Preparation of GO is easier compared to graphene (vi) GO could be dispersed much easily in a wide variety of polar solvents compared to graphene making TiO_2-GO composite preparation much easier [23,24].

Out of numerous methods of preparation of GO, the most widely adopted one is oxidation of graphene developed by Hummers and Offeman in 1958 [25]. Modified Hummers methods are commonly used nowadays. In this strategy oxidizing agents are penetrated between the layers of graphite resulting in the separation of GO layers and finally the oxidation reaction is terminated with the aid of H_2O_2 and water [26,27]. The mechanism of GO formation through three stages involving the formation of H_2SO_4-graphite intercalation compound followed by its oxidation and reaction with water was reported by A.M.Dimiev and J.M.Tour in 2014 [28] The advantages of GO preparation by Hummers/modified Hummers method are elimination of evolution of explosive gases and reduction of reaction time [29]. TiO_2 coupled with GO serves an efficient photocatalyst. The photogenerated electron in TiO_2 moves to the conduction band from where it is transferred to GO associated with it [30,31]. The electrons are well stabilized in GO network and interact with adsorbed oxygen forming O^- and O_2^- ions which are relayed to the reactant initiating various photochemical processes. The photo generated hole left behind interacts with adsorbed water forming hydroxyl radicals (-OH·) which further interacts with reactants leading to photochemical reactions [32].

2. Experimental

2.1. Materials

Polystyrene beads were purchased from LG Polymer India Pvt. Ltd, titanium dioxide (nano powder, 21 nm was purchased from Sigma Aldrich, graphite (150 mesh), sulphuric acid (98%), sodium nitrate, hydrogen peroxide (30% W/V),potassium permanganate and hydrochloric acid were purchased from Merk India. UV tube (253 nm. 30 W, Phillips Holland) fit inside a wooden chamber was used as UV light source. All the chemicals were used without further purification.

2.2. Synthesis of Graphene oxide(GO)

GO was synthesized by oxidation of graphite using modified Hummers method as presented in previous literatures [30,33].

2.3. Preparation of nano TiO_2 -graphene oxide (TiO_2-GO) photocatalyst

TiO_2-GO composites were prepared by sonication followed by hydrothermal process. TiO_2-GO composites with 1,3,10 and 30 weight percentages of GO namely TiO_2-1%GO, TiO_2-3%GO, TiO_2-10%GO and TiO_2-30%GO were prepared respectively. Inorder to prepare TiO_2-1%GO, 8mg of GO was dispersed in 80 ml water and 40 ml ethanol by through sonication using an ultrasonic probe sonicator (750 W) for two hours in a flask. 800 mg of nano TiO_2 was added to the flask and the sonication was continued for another two hours. The temperature of the flask was regulated using an ice bath inorder to prevent evaporation of solvents due to excess heating. The contents of the flask were transferred into a teflon lined hydrothermal autoclave which was kept in a hot air oven at a temperature 130°C for 6 hours. The bluesh grey solid powder hence obtained was filtered out from the solution and dried at 70°C for 12 hours. TiO_2-3%GO, TiO_2-10%GO and TiO_2-30%GO composites were prepared by the same route varying the weight percentages of GO taken [34,35].

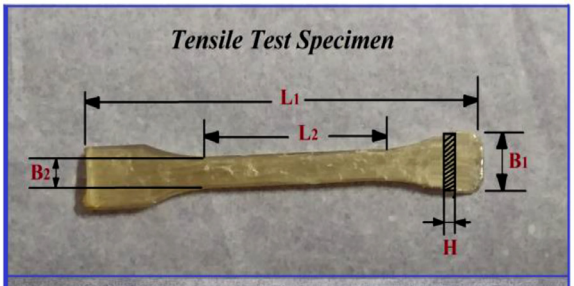

Tensile test specimen -Dimension-(ISO-527-2-1A)		
L1	Total length	75 mm
L2	Gauge length	30 mm
B1	Width of grip end	10 mm
B2	Width of center	05 mm
H	Thickness	02 mm
Flexural test specimen -Dimension-ISO-178		
L	Length	80 mm
B	Breadth	10 mm
H	Thickness	40 mm

Fig. 1. Dimensions of injection molded specimens for tensile and flexural measurements as per ISO standards.

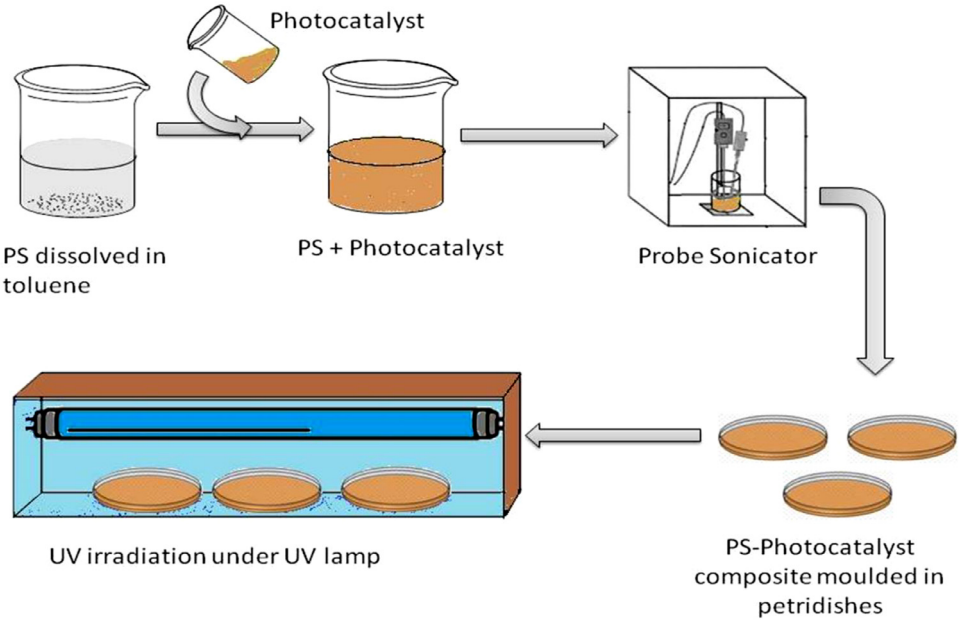

Fig. 2. Illustruction of PS composite preparation and their photodegradation setup.

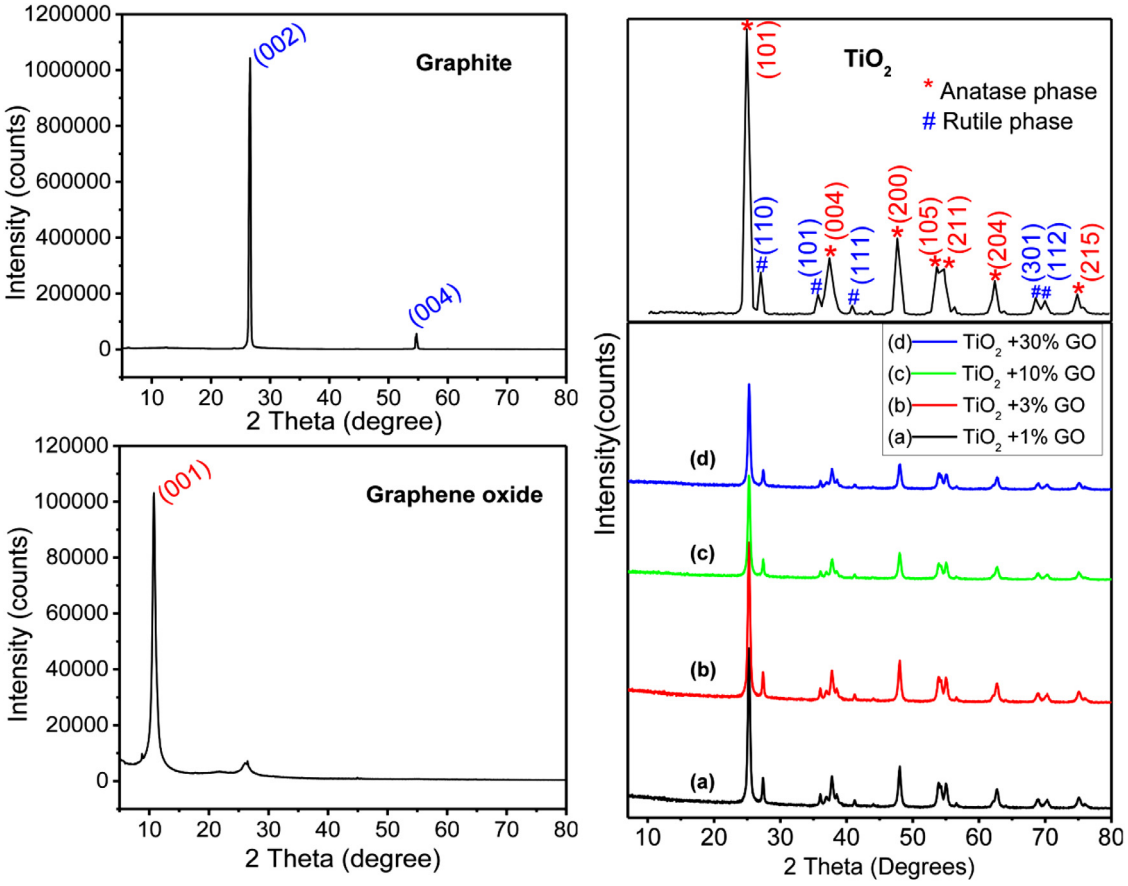

Fig. 3. Powdered XRD patterns of Graphite, GO, TiO_2 and TiO_2-GOcomposites.

2.4. Preparation of PS and PS-composite sheets

PS sheets were prepared through the method of solvent casting. Typically 5g of PS beads were dissolved in 20 ml toluene and the resulting viscous solution was sonicated using ultrasonic probe sonicator (750 W) for 30 minutes. The solution was immediately poured into petridishes of uniform dimensions and kept overnight in a vacuum oven. The obtained PS sheets were allowed to dry at room temperature for seven days. PS composite films were also casted through solvent casting method. Nano TiO_2 and TiO_2-GO photocatalysts were loaded into PS dissolved in toluene and the same process explained above was carried out. PS sheets and five different PS composite sheets namely PS-TiO_2, PS-TiO_2-1%GO, PS-TiO_2-3%GO, PS-TiO_2-10%GO, PS-TiO_2-30%GO were casted. The poly-

mer sheets were subjected to UV irradiation for photodegradation as explained in the forthcoming section.

2.5. Preparation of PS and PS composites for mechanical and electrical studies

Mechanical tests included determination of tensile and flexural properties. Polymer composites for mechanical studies were prepared by injection moulding technique. Finely chopped polymer flakes were fed into injection moulder (Windsor, India) which consisted of moulds corresponding to tensile and flexural test specimens. Dimension of polymer specimens for tensile test was as per ISO-527-2-1A standard while that of flexural was as per ISO-178 standard (Fig. 1). Electrical studies included dielectric breakdown (break down voltage) (BDV) measurement and determination of dielectric permittivity (εr) through capacitance measurement. Specimens for BDV were moulded by the aid of hydraulic hot press to obtain uniform discs of thickness 1 mm and diameter 75 mm. Polymer sheets were cut out into small circular button shaped discs of diameter 10mm for the determination of dielectric permittivity. The samples were then exposed to UV irradiation for photodegradation studies followed by mechanical and electrical testing.

2.6. Photodegradation reaction chamber

UV tube 30 W of wavelength 253 nm (Philips Holland) was fit inside a wooden chamber. The polymer specimens to be irradiated were kept at the base of the chamber over glass platforms. An exact distance of 8 cm was maintained between the specimens and the UV tube (Fig. 2). The irradiation was carried out continuously for 1000 hours. Inorder to nullify the errors caused by unpredictable power cuts, and weather changes all the specimens were irradiated at the same time. The specimens were subjected to various analyses at regular intervals of 200 hours.

2.7. Instrumentations

Powdered XRD analysis was done using X-Ray diffractometer, Aeris, PANalytical -with Copper-K alpha radiation (1.5406Å wavelength) as the source. Molecular weight determination was done using Gel Permeation Chromatography (GPC) LC-20AD, Shimadzu, Japan, with stationary phase silica gel and mobile phase tetrahydrofuran. IR spectroscopic studies were done using FTIR-ATR Spectrometer IRAffinity-1S, Shimadzu, Japan. UV-DRS analyses were conducted using UV-Visible spectrometer UV-26000, Shimadzu, Japan. SEM imaging was done using JSM-6390LV, JEOL. Energy dispersive X-Ray (EDX) analysis was done using OXFORD XMX N. HRTEM analysis was done using High resolution Transmission Electron Microscope JEM 2100, JEOL. Thermal studies were conducted in a thermogravimetric analyzer (TGA), STA 6000, PerkinElmer. Mechanical measurements were taken using universal testing machine (UTM), Autograph AG-X plus, Shimadzu. Raman spectroscopic analysis was done using a high resolution Raman spectrometer, Horiba JY. XPS analysis was done using XPS instrument, PHI 5000 Versaprobe Scanning ESCA Microprobe, Physical Electronics, USA. The photoluminescence (PL) and time resolved fluorescence spectral analysis were conducted using Fluoroscence Spectrometer with TCSPC, Fluorolog 3 TCSPC, Horiba, USA. The LED used was of 330 nm.

3. Results and Discussions

3.1. Characterization of Photocatalysts

Powdered XRD pattern of prepared GO exhibited its characteristic peak at an angle 2θ=10.7° corresponding to the (001) plane

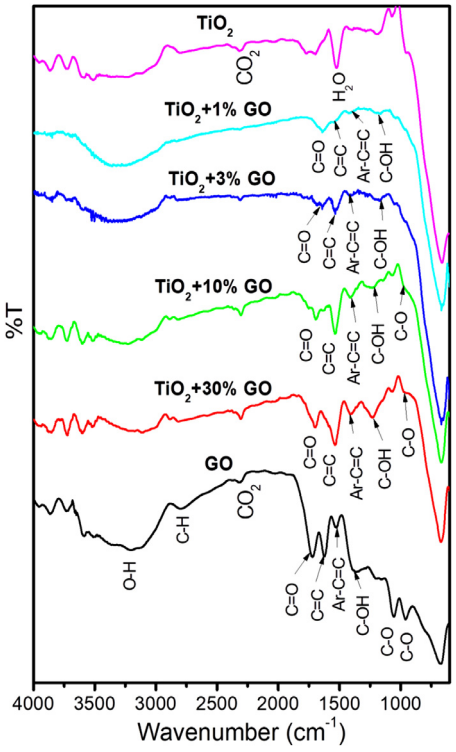

Fig. 4. FTIR spectra of TiO_2, GO and TiO_2-GO composites.

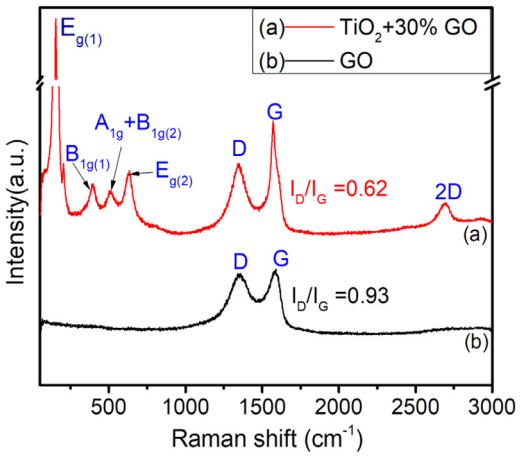

Fig. 5. Raman spectra of GO (a) and TiO_2-30%GO (b) composites.

of GO. In addition to this, broader peak of very low intensity was also observed at an angle 2θ=26°corresponding to the unoxidized graphite and/or reduced graphene oxide (rGO) present in traces (Fig. 3). The fact that pristine nano TiO_2 comprises predominantly anatase phase over rutile phase were quiet clear from the XRD pattern. The XRD patterns of TiO_2-GO exhibited all the peaks corresponding to TiO_2 with negligible shift in peak positions. All the peaks corresponding to TiO_2 in TiO_2-10% GO and TiO_2-30% GO composites showed a slight decrease in their peak intensities compared to that of pristine TiO_2, TiO_2-1%GO and TiO_2-3%GO reflecting the increased concentration of GO in the former composites. Peak sharpening were also observed in TiO_2-GO composites compared to pristine TiO_2 probably due to the increase in size of the composite particles with the incorporation of GO (Fig. 3). The peak observed at 2θ=10.7° for GO was invisible in TiO_2-GO composites. The reduction of GO, occurred during the hydrothermal process of TiO_2-GO composite preparation could be the possible reason for this observation (as evident from Raman spectroscopy and

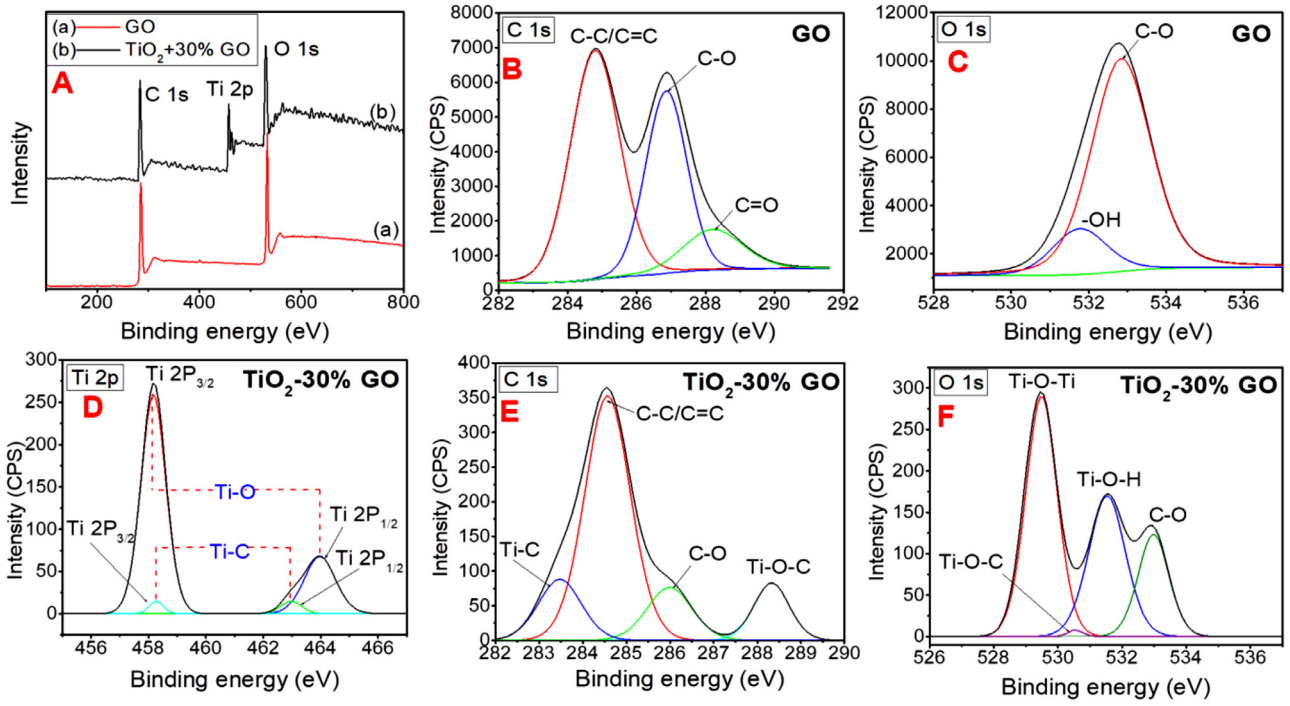

Fig. 6. XPS of GO and TiO_2-30%GO (a) and TiO_2-30%GO (b) composites.

Table 1
Highlighted peaks from FTIR spectra of GO and TiO_2-GO composites.

	GO	TiO_2+30%GO	TiO_2+10%GO	TiO_2+3%GO	TiO_2+1%GO
-C=0 (stretch)	1719 cm^{-1}	1699 cm^{-1}	1695 cm^{-1}	1645 cm^{-1}	1640 cm^{-1}
-C=C- (Stretch)	1622 cm^{-1}	1536 cm^{-1}	1536 cm^{-1}	1536 cm^{-1}	1536 cm^{-1}
Ar-C=C- (Stretch)	1519 cm^{-1}	1412 cm^{-1}	1410 cm^{-1}	1408 cm^{-1}	1408 cm^{-1}
-C-O-H (bend)	1377 cm^{-1}	1232 cm^{-1}	1224 cm^{-1}	1176 cm^{-1}	1165 cm^{-1}
-C-O- (Stretch)	1065 cm^{-1}	Overlapped by Ti-O stretching vibrational peaks.			
-C-O- (Stretch)	963 cm^{-1}	962 cm^{-1}	Overlapped by Ti-O stretching vibrational peaks.		

XPS analysis discussed below). The peak at 2θ=10.7° shifted to 2θ=26° corresponding to rGO in the TiO_2-GO composites. The inter planar distance (d) calculated using Bragg's equation showed a slight decrease for the TiO_2-GO composites compared to that of pristine TiO_2. Crystallite sizes calculated from Scherrer's formula was greater for TiO_2-GO composites as compared to pristine TiO_2 (refer supporting information table S1 and S2) [36].

FTIR spectra of GO exhibited its characteristic peaks which included –C=O (1719 cm^{-1}),-C=C- (1622 cm^{-1} and 1519 cm^{-1}), -C-O- (1065 cm^{-1} and 963 cm^{-1}), -OH (3600-3000 cm^{-1}) stretching, -C-O-H (1377 cm^{-1}) bending and -C-H (673 cm^{-1}) out of plane bending vibrations(Fig. 4). The presence of carboxylic acid and alcoholic functional groups in GO were hence quiet clear. FTIR spectra of TiO_2-GO composites exhibited characteristic vibrational peaks corresponding to TiO_2 as well as GO. A notable observation made from the IR spectra was that a considerable shift (towards lower wavenumber) in the peak positions occurred in TiO_2–GO composites when compared to GO. Among the composites as the percentage of GO incorporation increased, peaks corresponding to -C=O and -C-O-H functional group vibrations exhibited an observable shift in their positions. This observation suggested the existence of a strong interaction between TiO_2 and the oxygen atom of acid or alcoholic functional groups of GO. Increase in the intensities of IR absorption peaks of GO were also observed in the composites as the percentage of GO incorporation increased. Tabulated data of TiO_2-GO composites in comparison to GO is given in table 1.

Raman spectra of GO presented in Fig. 5a displays two bands at 1355 cm^{-1} (D band) 1587 cm^{-1} (G band). The D band represents the disorder of sp^3 carbon atom (having A_{1g} symmetry) where as G band could be attributed to the in-plane sp^2 carbon (E_{2g} symmetry) vibrational mode of graphene skeleton. The Raman spectra of TiO_2-30% GO (Fig. 5b) also shows D and G bands of graphene moiety. Bands observed at 154 cm^{-1}, 394 cm^{-1}, 511 cm^{-1} and 634 cm^{-1} could be attributed to $Eg_{(1)}$, $B_{1g(1)}$, A_{1g}+ $B_{1g(2)}$ and $E_{g(2)}$ respectively of anatase phase TiO_2 [37]. A band at 2695 cm^{-1} was also observed in TiO_2-30% GO composite that attributes the characteristic 2D band of sp^2 carbon of graphene (originating from two phonon double resonance). This band was however not observed in the spectra of GO. The appearance of 2D band reveals the presence of thin layers of exfoliated reduced GO associated with TiO_2 in the composite [33]. The ratio of intensities of D and G bands (I_D/I_G) calculated to be 0.93 in GO, decreased to 0.62 in TiO_2-30% GO. The decrease in the I_D/I_G value shows that some of the sp^3 bonds have been converted in to sp^2 (or decrease in structural defects with in sp^2 carbon) as a consequence of partial reduction of GO in TiO_2-GO composite [38].

The interaction between TiO_2 and GO in the TiO_2-GO composites was further clear from the XPS analysis of GO and TiO_2-30%GO (Fig. 6). XPS revealed the fact that partial reduction of GO has taken place in TiO_2-30%GO composites with the formation of Ti-C and Ti-O-C bonds, between TiO_2 and GO. Bands corresponding to C_{1S} and O_{1S} were observed in the XPS of GO and the bands corresponding to Ti_{2p}, C_{1S} and O_{1S} were observed in the XPS of TiO_2-

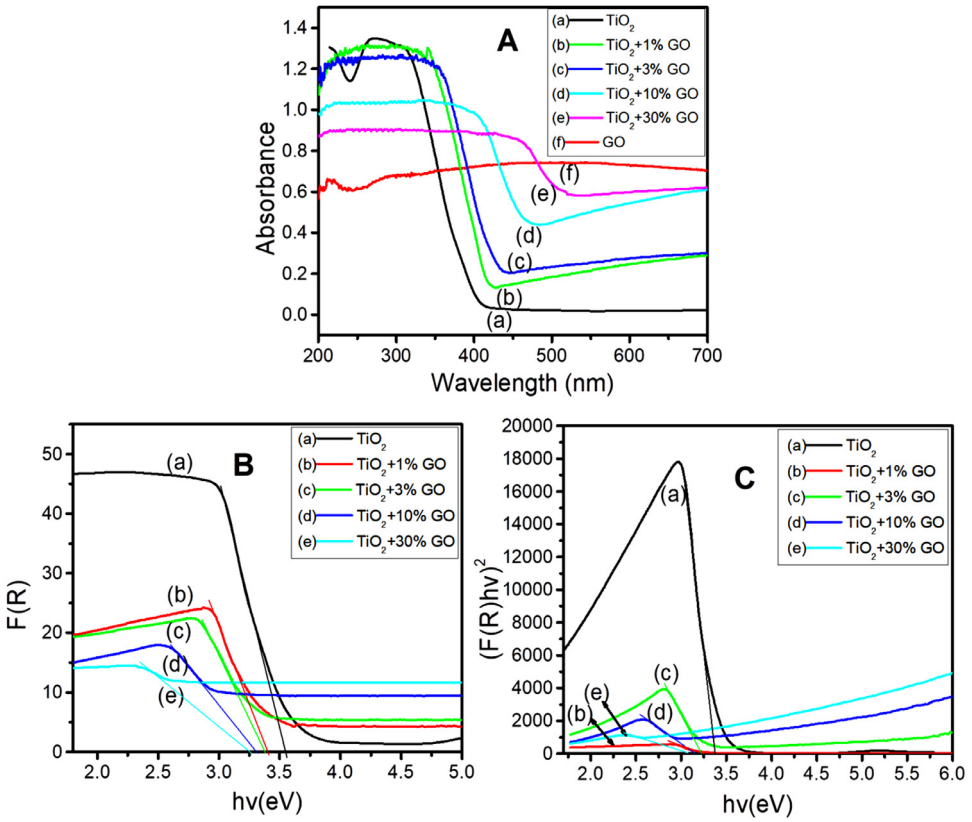

Fig. 7. UV DRS of TiO_2, GO and TiO_2-GO composites (A). Optical bandgap energy (Eg) determination of TiO_2 and TiO_2-GO composites (B and C).

30%GO (Fig. 6A). The deconvoluted spectra of C 1s region of GO exhibited three peaks corresponding to the binding energies 284.7 eV, 286.8 eV and 288.1 eV that could be assigned to C-C/C=C, C-O and C=O bonds respectively (Fig. 6B). C 1s region of TiO_2-30% GO composite (Fig. 6E) showed that the intensity of C-O binding energy peak decreased considerably compared to the C-O peak in C 1s region of GO. This is a clear evidence of partial reduction of GO. The C=O bond observed in GO was shifted to higher binding energy (288.5 eV) in TiO_2-30% GO composite due to the formation of Ti-O-C bond between TiO_2 and GO. A new peak centered at 283.4 eV represents Ti-C bond formed between TiO_2 and GO. The O 1s region of GO showed a peak centered at 532.9 eV representing –OH bond and a less intense peak at 531.8 representing C-O bond (Fig. 6C). O 1s region of TiO_2-30% GO composite displayed peaks centered at 529.4 eV, 530.5 eV, 531.5 eV and 532. 95 eV representing Ti-O-Ti, Ti-O-C, Ti-O-H and C-O bonds respectively (Fig. 6F). The deconvoluted spectra of Ti 2p region of TiO_2-30%GO composite gave four peaks (Fig. 6D). The peaks at 458.1 eV ($2p_{3/2}$) and 463.9 eV ($2p_{1/2}$) originated from the Ti-O bond existing in the composite. The low intensed peaks centered at 458.3 eV ($2p_{3/2}$) and 462.9 eV ($2p_{1/2}$) on the other hand originated from Ti-C bond in the composite [39–41]. The existence strong interaction between TiO_2 and GO that could facile easy transport of photogenerated charges between the composites was evident through XPS.

UV-visible spectra obtained from UV-DRS technique showed a decrease in the characteristic absorption band (UV region) of nano TiO_2 upon GO incorporation. A decrease in the UV absorption bands contradicted by the increase in the visible region absorption bands were observed as a consequence of increasing weight percentage of GO in TiO_2-GO composites (Fig. 7A). The visually observed bluish colouration of the TiO_2-GO composites could be seen as absorption bands in the visible region of UV-visible spectra. The origin of the bluish colour may be due to the reduction of some of the Ti^{4+} ions into Ti^{3+} ions during the process of GO incorporation. Interaction of TiO_2 with the π bonds of reduced graphene oxide could have caused this reduction [42]. Determination of optical band gap energies (E_g) of TiO_2 in comparison with TiO_2-GO composites was done by the application of Kubelka-Munk function (F(R)) (Equation 1) in Tauc method [43]. Reflectance spectra of the composites obtained through UV-DRS were used for E_g determination.

$$\text{Kubelka} - \text{Munk function } F(R) = \frac{(1-\mathrm{R})^2}{2\mathrm{R}} \quad (1)$$

Where R is the reflectance.

The extinction coefficient (α) used in Tauc method could be replaced by F(R) since F(R) is proportional to α (Equation 2).

$$F(R) = \frac{\mathrm{A}(h\upsilon - E_g)^n}{h\upsilon} \quad (2)$$

Where A is a constant and $h\upsilon$ represents the energy of photons.

The plote of F(R) against energy $h\upsilon$ in eV when extrapolated towards energy ($h\upsilon$) axis gave the E_g of the composites irrespective of the type of electronic transitions (direct or indirect transitions). The plotes $(F(R)h\upsilon)^2$ versus $h\upsilon$ where used to determine the E_gs corresponding to direct allowed electronic transition (Fig. 7 B&C). The later function which provided information about the types of transitions is termed as *modified Kubelka-Munk functions*. Modified Kubelka-Munk functions also holds further scope for determination of the E_gs corresponding to the other type of transitions just by substituting the exponential terms of $(F(R)h\upsilon)$ with their corresponding exponential factors which is insignificant in this piece of work. The value of E_g calculated through the two methods followed a common trend. The value of E_g of TiO_2 decreased as the percentage of GO incorporation increased (Table 2).

The photoluminescence (PL) spectra of TiO_2 (Fig. 8A) and TiO_2-30% GO (Fig. 8B) composite showed that the fluorescence emission

Table 2
Tabulated values of optical band gap energies of TiO_2 and TiO_2-GO composites.

Functions	Bang gap Energy in eV				
	TiO_2	TiO_2+1%GO	TiO_2+3%GO	TiO_2+10%GO	TiO_2+30%GO
F(R)	3.56	3.40	3.38	3.31	3.25
$(F(R)h\upsilon)^2$	3.38	3.25	3.22	3.15	3.07

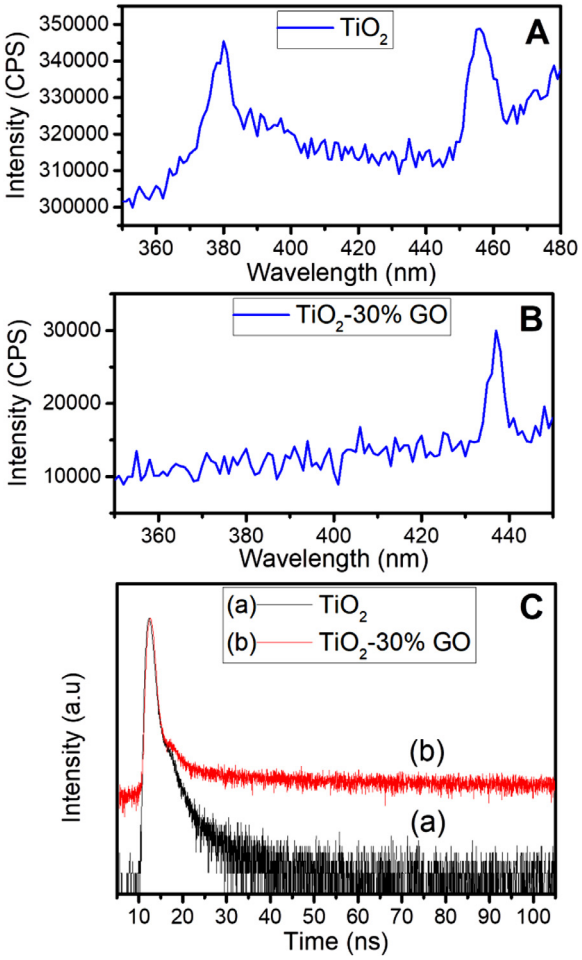

Fig. 8. PL spectra of TiO_2 (A), TiO_2-30%GO (B) and time-resolved fluorescence spectra of TiO_2 and TiO_2-30%GO (C) composite.

intensity of TiO_2-30% GO was lower compared to TiO_2. This observation discloses the fact that recombination of photo-generated electron-hole pair in TiO_2 was reduced when coupled with GO [44]. Time-resolved fluorescence spectra (TCSPC) of the TiO_2 and TiO_2-30% GO (Fig. 8C) further proved that the recombination rate of charge carriers decreased in TiO_2-30% GO compared to pristine TiO_2. The average life time $<\tau>$ was calculated from the expression below (equation 3) by fitting the decay curve using triple exponential function [45].

$$\langle\tau\rangle = \left(A_1\tau_1^2 + A_2\tau_2^2 + A_3\tau_3^2\right)/(A_1\tau_1 + A_2\tau_2 + A_3\tau_3) \quad (3)$$

Where, τ_1, τ_2 and τ_3 are the life times corresponding to the amplitudes A_1, A_2 and A_3.

The average lifetime of TiO_2-30%GO composite (1.37 ns) was found to be higher than that of pristine TiO_2 (0.87 ns). The increased fluorescence life time observed in TiO_2-30%GO reveals better separation of charge carriers in the composite due to the transfer of electrons from TiO_2 to GO.

SEM image revealed that the prepared TiO_2-GO composites existed as nano particles (Fig. 9A). The presence of titanium (15.92 at%), oxygen(50.93 at%) and carbon (33.15 at %) were detected through EDX technique for TiO_2-3%GO composite without the presence of any other impurities (Fig. 9B). HRTEM image revealed that the TiO_2-GO composite existed as separated particles rather than sheets or any other amorphous forms. GO seemed to have broken down into thin sheets of nano dimensions (Fig. 9C). Ultra sonication followed by hydrothermal process might have caused the sheets to break up into such nano dimensions. Lattice fringes with a spacing of 0.35 nm assigned to TiO_2 anatase (101) planes could be visualised HRTEM image (Fig. 9D). Selected area electron diffraction (SAED) pattern revealed the crystalline nature of the composite (Fig. 9E). Points corresponding to (101), (200) and (105) planes of anatase phase and (101), (111) planes of rutile phase TiO_2 were spotted from SAED patterns. The results were in well agreement with powdered XRD patterns. Average particle size (TiO_2 ≈23 nm and TiO_2-3%GO ≈ 44 nm) were determined from the TEM image through *image j* software (Fig. 9F).

3.2. Monitoring the Photodegradation of PS

PS, PS-TiO_2 and PS-TiO_2-GO composites were subjected to GPC measurements after regular intervals (200 hours) of UV irradiation. The average molecular weights were determined using GPC and using these data, polydispersity index (PDI), chain scission per macro molecule (S) and number of scission events per gram (N_t) of PS were determined using the equations given below Equations 4,5 and (6). Tabulated data obtained from GPC analysis representing M_w, M_n, PDI, S and N_t is given in supporting information (Table S3).

$$PDI = \frac{M_w}{M_n} \quad (4)$$

$$S = \frac{(Mn)_0}{(Mn)_t} - 1 \quad (5)$$

$$Nt = \frac{1}{(Mn)_t} - \frac{1}{(Mn)_0} \quad (6)$$

Where Mn and Mw represents number and weight average molecular weight of PS respectively;

$(Mn)_0$ and $(Mn)_t$ represents number average molecular weight before and after *t* hours of UV irradiation respectively.

Decrease in average molecular weights (number average (Mn), weight average (Mw) and Z- average (Mz) molecular weights) were observed for PS as well as PS composites as a consequence of UV irradiation (Fig. 10A). The polymer specimens showed a decrease in their average molecular weights when measured at different intervals of increasing UV irradiation time. Molecular mass loss was most predominant in PS-(TiO_2+30%GO) composite compared to the other specimens under study. The decrease in molecular mass of the polymers could be attributed to the polymer chain breakage which inturn was a consequence of polymer degradation on UV exposure. The increase in the values of *S* and N_t reveled the fact that irregular chain scission of the polymer specimens had taken place upon UV irradiation (Fig. 10C & D). Increase in PDI of

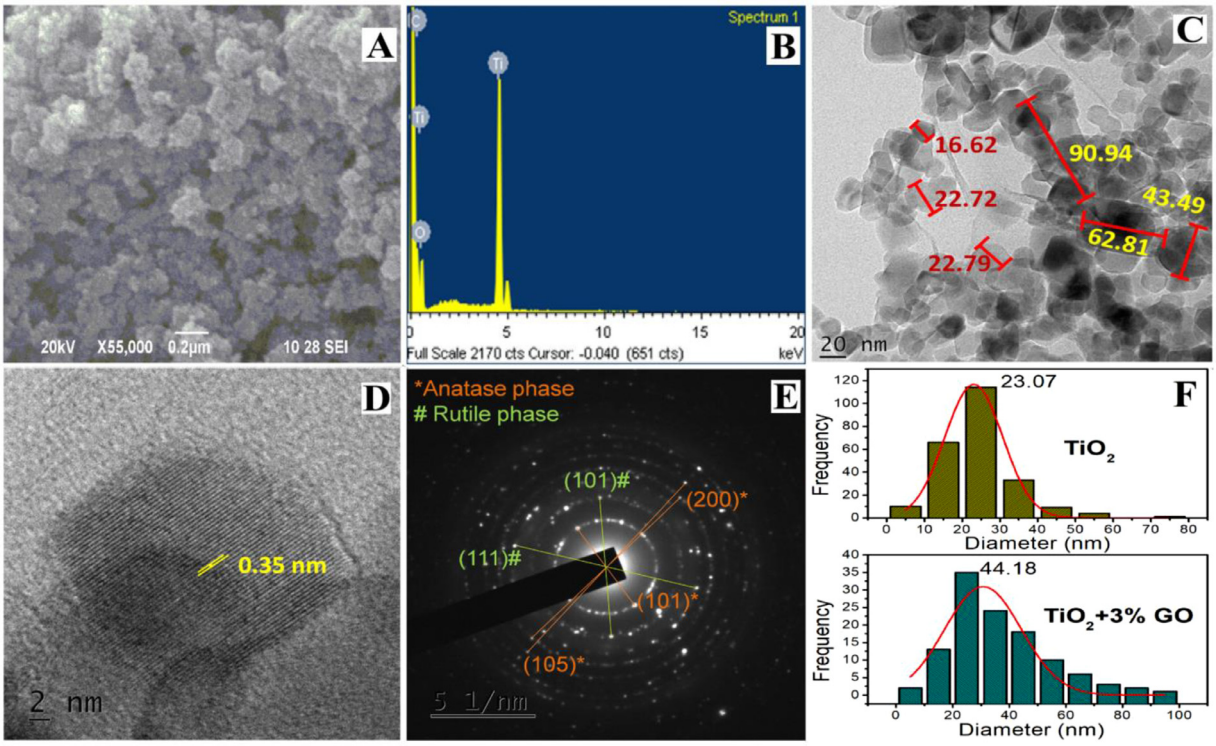

Fig. 9. SEM image (A), EDX (B), HRTEM image (C & D), SAED pattern (E) and particle size distribution histogram (F) of TiO_2-3% GO composite.

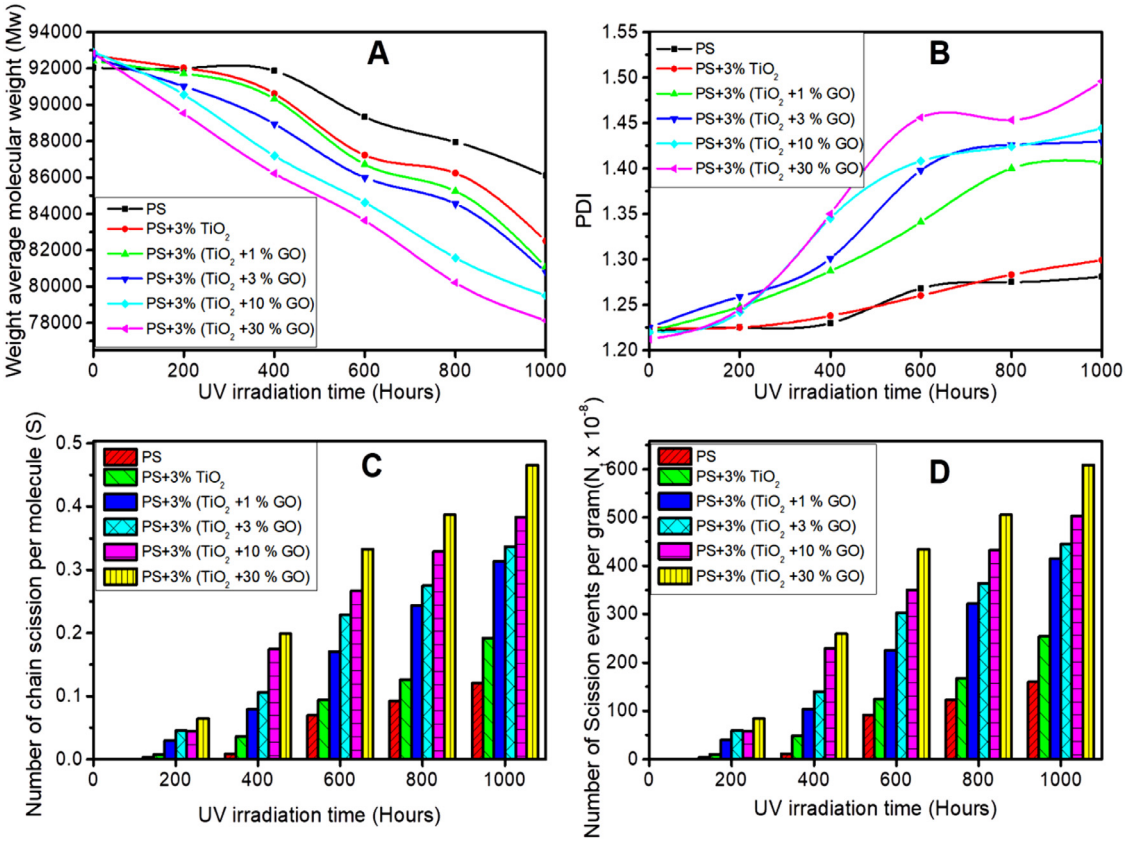

Fig. 10. Mw (A),PDI (B), number of chain scission per molecule, S (C) and number of scission events per gram, N_t (D) of PS, PS-TiO_2, and TiO_2- GO composites as determined through GPC.

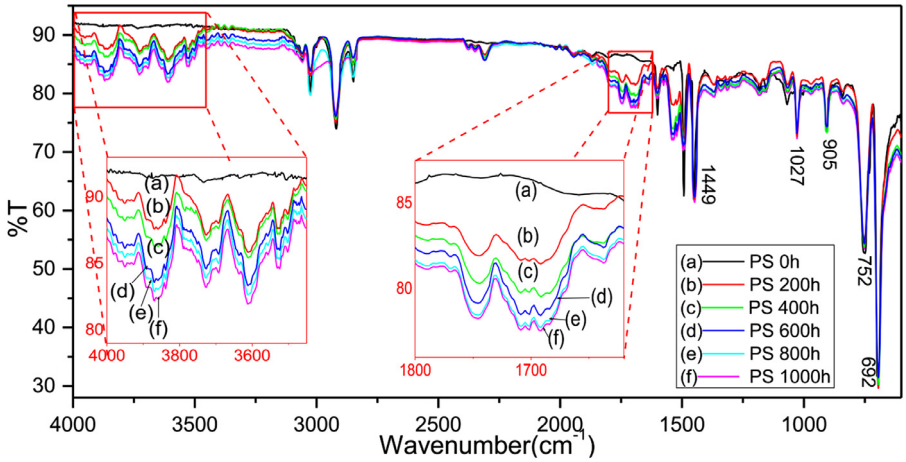

Fig. 11. FTIR spectra of PS after different UV exposure time intervals ranging from 0h to 1000h.

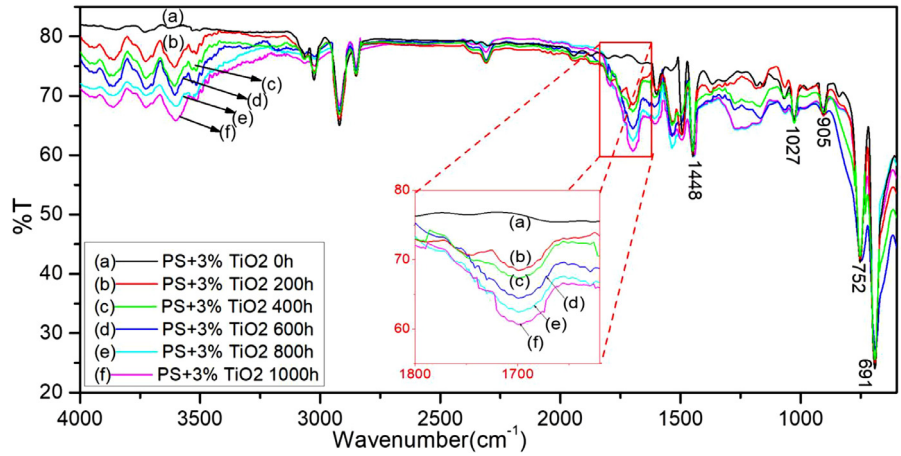

Fig. 12. FTIR spectra of PS-3%TiO_2 after different UV exposure time intervals ranging from 0h to 1000h.

the composites further elucidates that the chain breakage was irregular which lead to the formation of macromolecules of varying molecular massed (Fig. 10B). It was clear from GPC data that PS-TiO_2-GO composites underwent better chain breakdown compared to PS-TiO_2 composites.

The change in chemical structures of the polymer specimens were investigated through FTIR spectroscopy. For the PS and PS composites under study it was found that the intensities of peaks corresponding to carbonyl (C=O), hydroxyl (-OH)/ hydroperoxy (-OOH), carbon- carbon double bond (C=C) etc stretching vibration has increased with respect to UV irradiation time. The characteristic bands corresponding to phenyl rings of the specimens on the other hand showed no much observable change probably because the rings remained intact on UV exposure. From the FTIR spectra of PS (Fig. 11), formation of new bands between the ranges 4000-3500 cm^{-1}, 1740-1680 cm^{-1}, 1680-1650 cm^{-1} and 1630-1600 cm^{-1} was observed upon UV irradiation for 200h which could be attributed to –OH /-OOH, carbonyl –C=O, alkenic -C=C- and conjugated carbon double bond stretching frequencies respectively. Increase in the absorption intensities of these bands could also be seen as the time of UV irradiation increased. Peaks at 1449, 1027,905,752 and 692 cm^{-1} corresponding to out of plane C-H bend of phenyl rings remained unaltered upon UV irradiation. Similar observations were made for PS-TiO_2 (Fig. 12) as well as PS-TiO_2-GO composites (Fig. 13) under UV irradiation. It was found that the increase in the above mentioned absorption bands were maximum for PS-(TiO_2-30%GO) composite. Accounting all the observations made from FTIR spectra, it could be concluded that photo-oxidation have taken place for the polymer composites upon UV irradiation. Predominant oxidation was identified in PS-(TiO_2-30%GO) composite. FTIR spectra of PS-(TiO_2-1%GO), PS-(TiO_2-3%GO), PS-(TiO_2-10%GO) is given in supporting information (Figure S1, S2 and S3).

UV-visible spectra (UV DRS) of pristine PS as well as PS composites under study showed notable changes in their characteristic absorption bands upon UV exposure (Fig. 14A, B &C). An appreciable decrease in the absorption peaks of the polymer specimens were observed in the UV region (between 230-400 nm) with respect to the increase in irradiation time. This observable hypochromic effect reflected the degradation of polymer chain. As evident from FTIR spectra explained above the increase in –C=O ($n\rightarrow\pi^*$) absorption bands with UV exposure time could not be identified over this area (230-290 nm) due to their low intensity. The depletion of polymer chain lead to a decrease in the absorption bands predominating the formation of –C=O groups which should otherwise have caused an increase in intensity (due to $n\rightarrow\pi^*$ transition) over this area (230-290 nm). The region of UV spectra with wavelength below 230 nm showed an increase in the absorption bands with respect to UV irradiation time. This hyperchromic effect could be due to the increase in the absorption

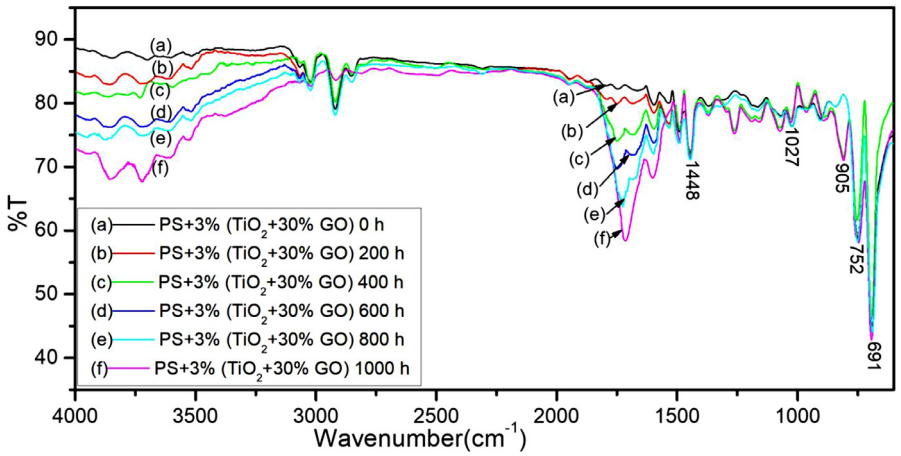

Fig. 13. FTIR spectra of PS-3%(TiO_2-30% GO) after different UV exposure time intervals ranging from 0h to 1000h.

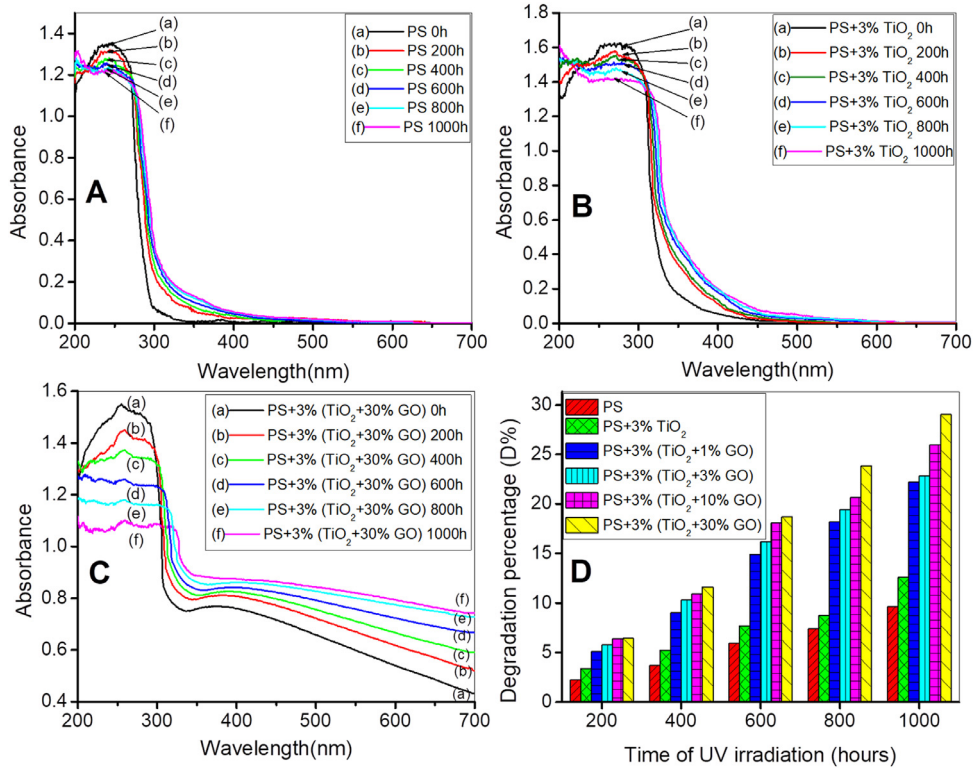

Fig. 14. UV-Visible spectra of PS (A), PS-3%(TiO_2) (B), PS-3%(TiO_2-30% GO) (C) and degradation percentages of PS, PS-TiO_2 & PS-TiO_2-GO (D) after different UV exposure time intervals ranging from 0h to 1000h.

bands of -OH (n→π^*), -C=O (π →π^*) and -C=C- (π →π^*) functional groups upon irradiation. Another striking trend observable from the UV-Vis spectra was an increased bathochromic shift (red shift) and increase in intensity in the visible region with respect to the irradiation time for all specimens. Formation and increase in conjugated double bonds between carbon atoms was evident from this observation. The observable trends as mentioned above of UV DRS were predominant in PS-(TiO_2-30%GO) composites.

The percentages of photodegradation (D%) at each time interval of UV irradiation were calculated using equation 7 from the UV-Visible spectra.

$$D\% = \left(\frac{A_0 - A}{A_0}\right) X100 \tag{7}$$

Where A_0 and A represents the absorption maxima of the polymer specimens before and after UV irradiation respectively.

D% was found to be higher for PS-TiO_2-GO composites. Maximum D% was obtained for PS-(TiO_2 +30% GO) composite (Fig. 14 D).

Optical band gap energy (E_g) of PS, PS-TiO_2 and PS-TiO_2-GO films before and after UV irradiations of different intervals were determined using Tauc relation (Equation 8)

$$\alpha h\upsilon = A(h\upsilon - E_g)^n \tag{8}$$

Were E_g represents the band gap energy, α represents the absorption coefficient, $h\upsilon$ represents the energy of photon in eV, *A* and *n* are constants which depends upon the type transitions (direct, indirect etc).

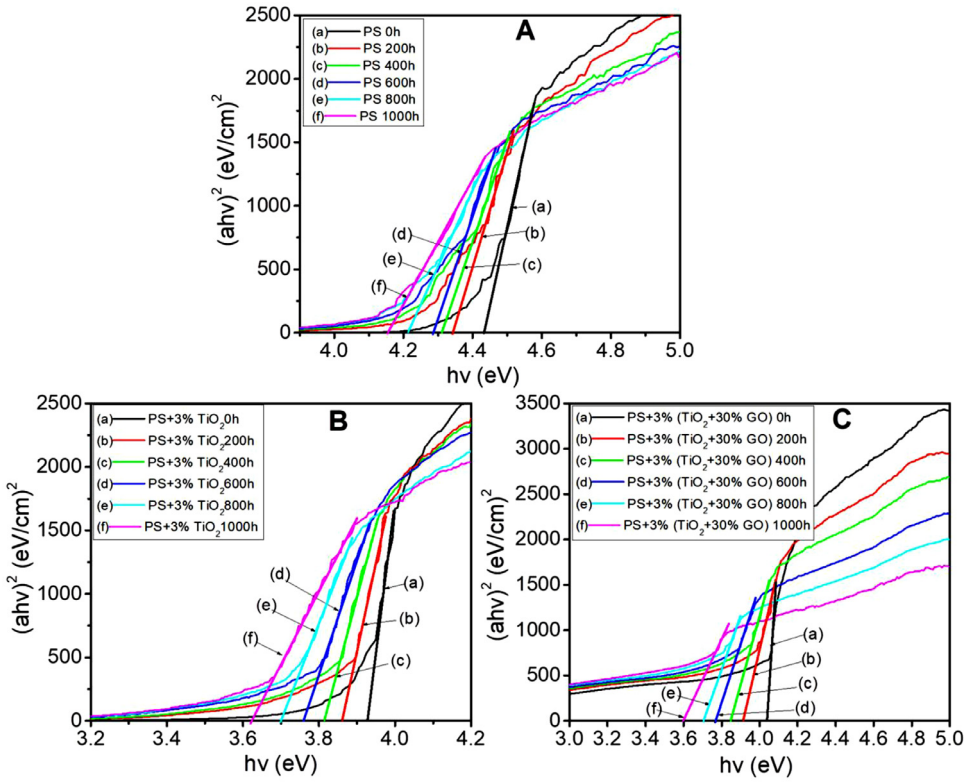

Fig. 15. Optical bandgap energy determination from the plot of $(\alpha h\upsilon)^2$ v/s $h\upsilon$ for PS (A), PS-3%(TiO_2) (B) and PS-3%(TiO_2-30% GO) (C) subjected to different UV exposure time intervals ranging from 0h to 1000h.

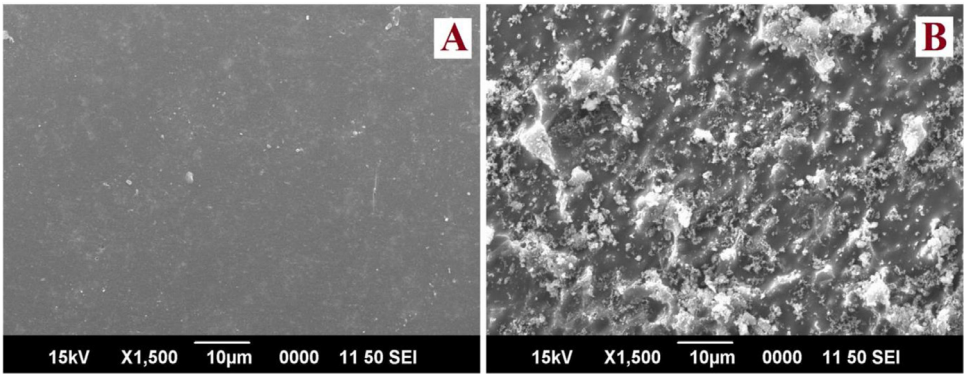

Fig. 16. SEM image of PS-3%(TiO_2-30%GO) composite before (A) and after (B) UV irradiation of 1000 h.

The plote $(\alpha hv)^2$ versus hv was used to determine the direct allowed E_g. The values of E_g for the polymer specimens under study decreased as the time of UV irradiation increased (Fig. 15).

SEM image revealed the increase in surface roughness of PS composites after UV exposure. Fig. 16 shows the SEM image of PS-3%TiO_2 composite before and after UV exposure of 1000 hours.

3.3. Electrical properties of PS and PS composites

Dielectric breakdown (Break down voltage) of the polymer samples measured in alternating current of frequency 50Hz is as illustrated in Fig. 17. The break down voltage (BDV) of PS before UV irradiation was determined to be 25.17 KV/mm. The BDV of PS-TiO_2 composites showed an increased value of 30.03 KV/mm. The percentage of GO incorporation decreased the BDV of the composites due to conductive nature of GO. PS composites with 3%, 10% and 30% GO incorporated TiO_2 exhibited BDV values lower than pristine PS. The dielectric breakdown of all the specimens decreased upon UV irradiation. The decrease in BDV with respect to UV irradiation time could be attributed to the formation of charge centers due to photodegradation. The charge centers formed along the polymer chain lead to the flow of electric current much easier through the polymer chains resulting in a decreased BDV. Decrease in the BDV upon UV irradiation was predominant in PS-TiO_2-30% GO composite compared to the other specimens under study.

Dielectric permittivity (ε_r) of the polymer specimens were calculated from their determined capacitance value using equation 9.

$$C = \varepsilon_r\ \varepsilon_0\ \left(A/t\right) \tag{9}$$

Were,

C = Capacitance; ε_r = dielectric permittivity; ε_0 is the dielectric permittivity of free space (8.854 × 10−12 F/m); A is the area and t is the thickness of the polymer specimens.

The composites (PS-TiO_2 and PS-TiO_2-GO) exhibited a better dielectric permittivity (ε_r) compared to that of pristine PS

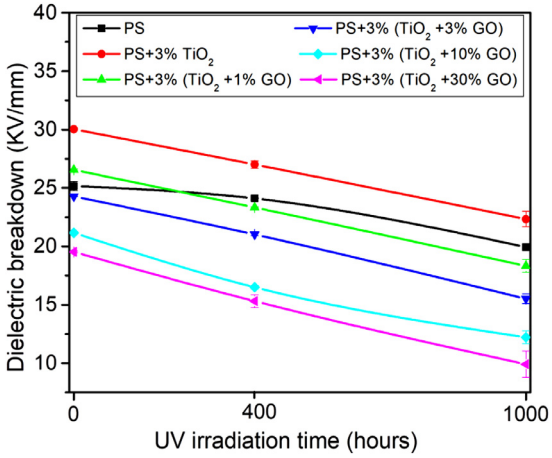

Fig. 17. Dielectric break down of PS, PS-TiO_2 and PS-TiO_2-GO composites exposed to UV radiation for 0,400 and 1000 h.

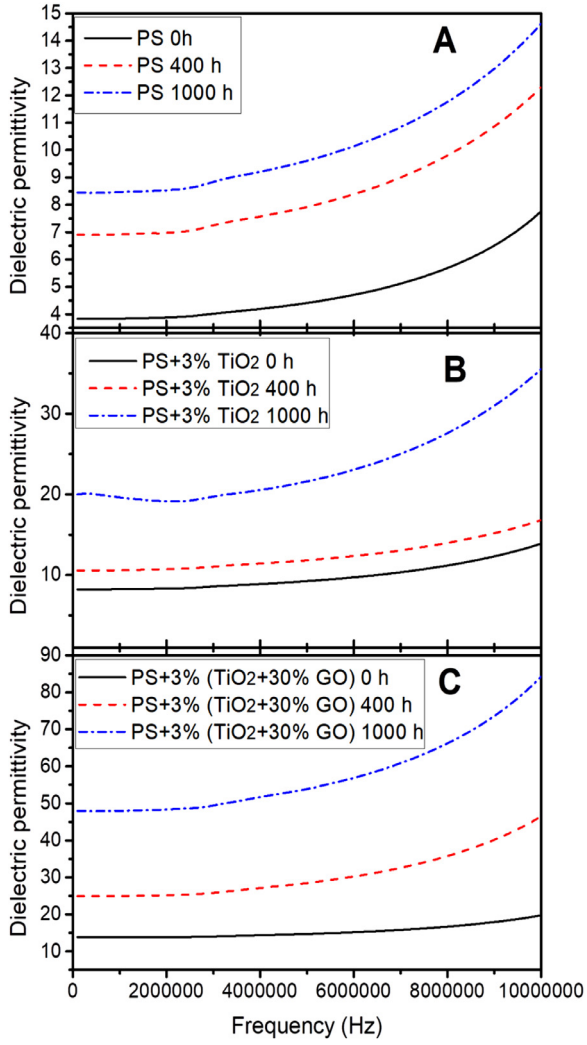

Fig. 18. Dielectric permittivity of PS (A), PS-3%TiO_2 (B) and PS-3%(TiO_2-30%GO) (C) composites exposed to UV radiation for 0,400 and 1000 h.

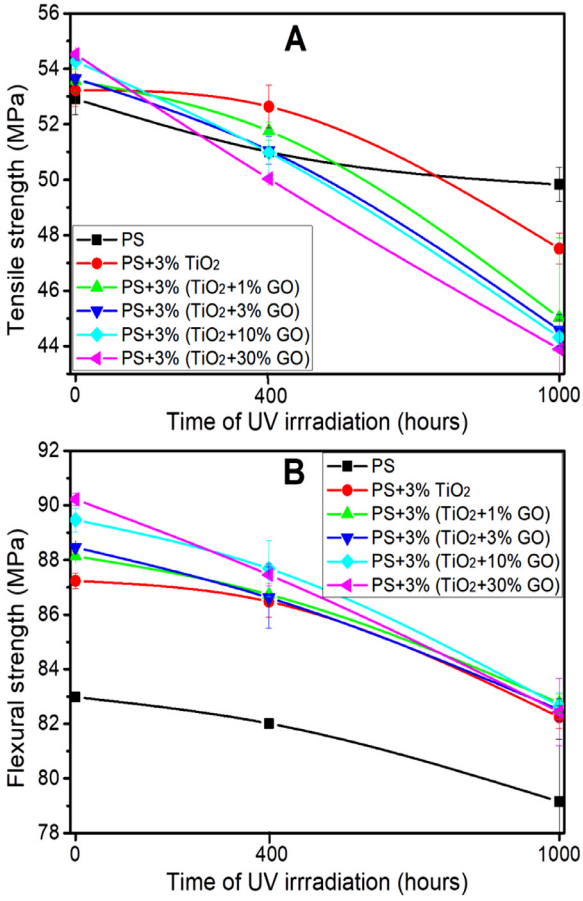

Fig. 19. Tensile (A) and flexural (B) strengths of PS, PS-TiO_2 and PS-TiO_2-GO composites exposed to UV radiation for 0,400 and 1000 h.

(Fig. 18). The ε_r of PS as well as PS composites increased upon UV irradiation. The formation of charge centers as a result photodegradation of PS resulted to an increase in ε_r which could most predominantly be seen in PS-TiO_2-30%GO composite compared to the other specimens.

3.4. Mechanical properties of PS and PS composites

PS composites showed enhanced tensile as well as flexural properties compared to pristine PS. The superior mechanical properties demonstrated by PS nano composites over pristine PS promises the scope of their wide application in various sectors. The tensile and flexural strengths of PS, PS-TiO_2 and PS-TiO_2-GO decreased as the time of UV irradiation increased (Fig. 19 A & B). Depletion of mechanical property as a consequence of chain degradation is clearly understood here.

3.5. Thermal properties of PS and PS composites

From the TGA thermogram it was found that the glass transition temperature (Tg) of PS composites were higher compared to that of pristine PS (Fig. 20). The Tg for PS observed at a temperature above 117.8°C increased to 130.2°C for PS+30% TiO_2 composite and to 140.5°C for PS+3%(TiO_2+30% GO) composite. The decomposition temperature of PS observed at 251.5-393.9°C also increased for the PS composites (271.5-407.2°C for PS+30% TiO_2 and 320-437.6°C for PS+3% (TiO_2+30% GO) composite). The Tg as well as decomposition temperature of UV irradiated PS and PS composites decreased appreciably compared to their unirradiated counterparts. UV irradiation of the PS and PS composited lead to the breakage or weak-

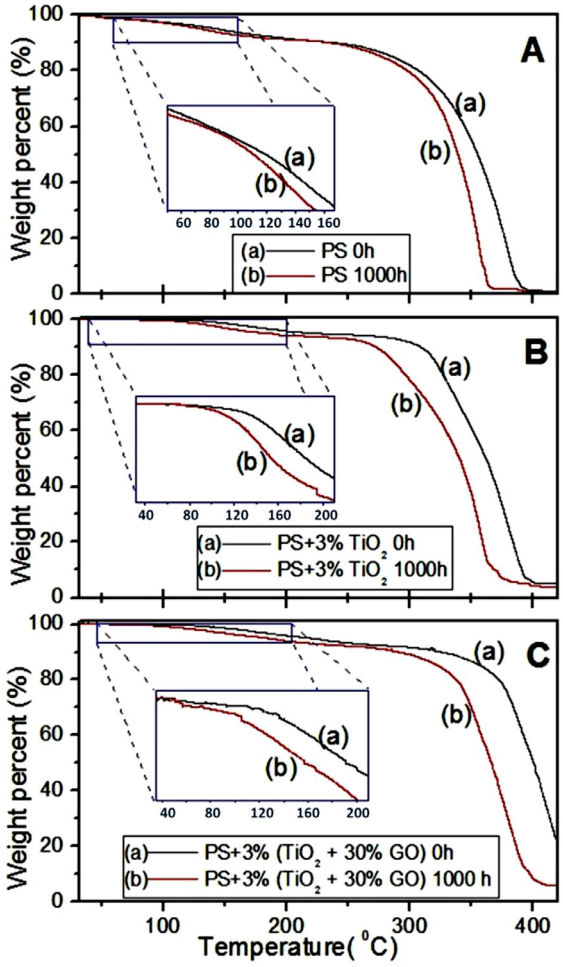

Fig. 20. TGA thermogram of PS (A), PS-3%TiO_2 (B) and PS-3% (TiO_2-30%GO)(C) composites before and after UV irradiation of 1000 h.

ening of their polymer chains resulting in the decrease of Tg and decomposition temperature.

3.6. Mechanism of Photodegradation

As reported in our previous work the mechanism of photodegradation is initiated when the phenyl rings of PS chain absorbs UV radiation and get excited to singlet state followed by triplet state through inter system crossing [46]. Cleavage of -C-C- bonds and -C-H bonds take place at this stage through radical mechanism. The radicals are propagated through the polymer resulting in polymer chain break down (as evident from GPC), formation of carbon-carbon double bonds and conjugated double bonds (as evident from FTIR). The macromolecular radicals also interact with adsorbed water leading to the formation of C–OH groups on the polymer chain while the interaction of radicals with adsorbed oxygen leads to the formation of carbonyl bonds (-C=O) on the polymer chain (Evident from FTIR). It was observed that the degradation of PS was accelerated in the presence of TiO_2 and TiO_2-GO photocatalysts. GO incorporation increased the photocatalytic efficiency of TiO_2. The life time of photogenerated charge carriers was found to be longer in TiO_2-GO (evident from TCSPC), suggesting better separation of charge carriers in the composites compared to pristine TiO_2. Partial reduction of GO has taken place in TiO_2-GO composites (evident from Raman spectroscopy and XPS analysis). The photo generated electrons can be transferred from the conduction band of TiO_2 to the partially reduced GO (rGO) which acts as electron sink, associated with TiO_2, minimising charge recombination. The charge transport through the TiO_2-GO heterojunctions is further assisted by the Ti-O-C and Ti-C bond bridges formed between TiO_2 and GO (evident from Raman spectroscopy). The electrons transferred into GO from TiO_2 can further react with adsorbed oxygen to create superoxide anion ($O_2^{\cdot -}$). Meanwhile the holes left behind in the valence band of TiO_2 reacts with adsorbed water molecules forming -OH·. These radicals interact with PS accelerating its photodegradation until the UV light source is removed and all the radicals are quenched.

3.7. Eco friendliness in TiO_2-GO catalysed photodegradation of PS and relevance of this investigation

- Photodegradation occurs under direct sunlight without the requirement of extra energy making the process costless.
- No toxic gases are liberated during the process.
- TiO_2 and GO are non-hazardous materials.
- Loading optimum amount of GO-TiO_2 makes PS mechanically strong and thermally more stable promising wide range of applications.
- GO-TiO_2 catalysed photodegradation of PS were established to be more efficient compared to TiO_2 catalyst.
- Association of GO over the surface of TiO_2 allows their dispersion much easier in water. This property could be utilized in the degradation of PS spread over water bodies.

4. Conclusion

Preparation of nano TiO_2-GO photocatalysts was successfully done through sonication assisted hydrothermal process. The formation of nano sized GO sheets associated with nano TiO_2 was evident from various characterization techniques used. The shift in peak positions as observed from FTIR spectra made it clear that a strong interaction existed between TiO_2 and GO. The optical band gap energy of TiO_2 decreased as the percentage of GO added to TiO_2 increased. Raman spectra and XPS analysis proved that partial reduction of GO took place in TiO2-GO composites. Existence of Ti-O-C and Ti-C bonds between TiO_2 and GO was evident from XPS. The charge carrier life time determined through TCSPC analysis was found to be longer in TiO_2-GO compared to pristine TiO_2. HRTEM and SAED pattern served an important tool for the identification of TiO_2-GO morphology which revealed that the particles were nano sized and crystalline. TiO_2-GO catalysed photodegradation of PS was compared with that of pristine PS and PS-TiO_2 composite. The decrease in average molecular weights, increase in chain scission and increase in polydispersity index as analysed through GPC highlighted the fact that the polymer specimens underwent random chain scission upon UV irradiation. FTIR spectra revealed the fact that polymer chains had underwent photo oxidation when exposed to UV radiation. Decrease in mechanical strengths upon UV irradiation suggested deterioration of the polymer chain due to bond rupture occurred in the polymer chain. Decrease in dielectric strength and increase in dielectric permittivity pointed out the formation of charge centers and polar groups upon UV irradiation. The shift in decomposition temperature and glass transition temperature towards lover value further supported the deterioration in the polymer chain due to bond cleavage as a consequence of photodegradation under UV irradiation. It was confirmed from all the analytical data and measurements that photodegradation of PS loaded with TiO_2-GO composite took place in a more accelerated way compared to that of pristine PS and PS-TiO_2 composites. The fact that TiO_2-GO composite served an efficient photocatalyst for the photodegradation of PS was hence concluded. From the investigations conducted the

order of photodegradation of PS composites upon photodegradation was found to obey the following order; PS-(TiO_2+30%GO)> PS-(TiO_2+10%GO)> PS-(TiO_2+3%GO)> PS-(TiO_2+1%GO)> PS-TiO_2> PS. TiO_2-GO photocatalysed degradation of PS under UV irradiation hence proved to be an effective method for eradication of PS debris. Both GO and TiO_2 being non hazardous, they promise an ecofriendly approach for the degradation of PS wastes.

CRediT Author Statement

1 **Dinoop lal S**: Conceptualization, formal analysis, investigation, data curation, roles/writing - original draft, methodology, software, acquisition, visualization
2 **Sunil Jose T**: conceptualization, project administration, supervision, writing - review & editing, data curation, methodology, acquisition, visualization
3 **Rajesh C**: resources, conceptualization, acquisition, validation
4 **Arun K J**: resources, software, validation

Declaration of Competing Interest

The authors declare that they have no known competing financial interests or personal relationships that could have appeared to influence the work reported in this paper.

Aknowledgement

The authors are thankful to SAIF-STIC, Cochin University of Science and Technology, India, National Institute of Technology, Calicut, India and CSIR-Central Electrochemical Research Institute, Karaikudi, India, CSIR-NIIST Trivandrum, India and MG University Trivandrum, India for their valuable support.

References

[1] T. Takasuga, T. Makino, K. Tsubota, N. Takeda, Formation of dioxins (PCDDs/PCDFs) by dioxin-free fly ash as a catalyst and relation with several chlorine-sources, Chemosphere 40 (2000) 1003–1007, doi:10.1016/S0045-6535(99)00345-8.
[2] G.Q. Ali, G.A. El-Hiti, I.H.R. Tomi, R. Haddad, A.J. Al-Qaisi, E. Yousif, Photostability and Performance of Polystyrene Films Containing 1,2,4-Triazole-3-thiol Ring System Schiff Bases, Molecules 21 (2016), doi:10.3390/molecules21121699.
[3] B. Gewert, M. Plassmann, O. Sandblom, M. MacLeod, Identification of Chain Scission Products Released to Water by Plastic Exposed to Ultraviolet Light, Environ. Sci. Technol. Lett. 5 (2018) 272–276, doi:10.1021/acs.estlett.8b00119.
[4] E. Yousif, R. Haddad, Photodegradation and photostabilization of polymers, especially polystyrene: review, Springerplus 2 (2013) 1–32, doi:10.1186/2193-1801-2-398.
[5] Y. Lei, H. Lei, J. Huo, Innovative controllable photocatalytic degradation of polystyrene with hindered amine modified aromatic polyamide dendrimer/polystyrene-grafted-TiO2 photocatalyst under solar light irradiation, Polym. Degrad. Stab. 118 (2015) 1–9, doi:10.1016/j.polymdegradstab.2015.04.005.
[6] R. Vijayalakshmi, V. Rajendran, Synthesis and characterization of nano-TiO2 via different methods, Arch. Appl. Sci. Res. 4 (2012) 1183–1190.
[7] M. Sachs, E. Pastor, A. Kafizas, J.R. Durrant, Evaluation of Surface State Mediated Charge Recombination in Anatase and Rutile TiO2, J. Phys. Chem. Lett. 7 (2016) 3742–3746, doi:10.1021/acs.jpclett.6b01501.
[8] M.B. Suwarnkar, R.S. Dhabbe, A.N. Kadam, K.M. Garadkar, Enhanced photocatalytic activity of Ag doped TiO2 nanoparticles synthesized by a microwave assisted method, Ceram. Int. 40 (2014) 5489–5496, doi:10.1016/j.ceramint.2013.10.137.
[9] S. Bagheri, D. Ramimoghadam, A.T. Yousefi, S.B.A. Hamid, Synthesis, characterization and electrocatalytic activity of silver doped-titanium dioxide nanoparticles, Int. J. Electrochem. Sci. 10 (2015) 3088–3097.
[10] M.B. Marami, M. Farahmandjou, B. Khoshnevisan, Sol-Gel Synthesis of Fe-Doped TiO2 Nanocrystals, J. Electron. Mater. 47 (2018) 3741–3748, doi:10.1007/s11664-018-6234-5.
[11] J. Tian, L. Chen, Y. Yin, X. Wang, J. Dai, Z. Zhu, X. Liu, P. Wu, Photocatalyst of TiO2/ZnO nano composite film: Preparation, characterization, and photodegradation activity of methyl orange, Surf. Coatings Technol. 204 (2009) 205–214, doi:10.1016/j.surfcoat.2009.07.008.
[12] D. Robert, Photosensitization of TiO2 by MxOy and MxSy nanoparticles for heterogeneous photocatalysis applications, Catal. Today. 122 (2007) 20–26, doi:10.1016/j.cattod.2007.01.060.
[13] P.V Kamat, D. Meisel, Nanoscience opportunities in environmental remediation, Comptes Rendus Chim 6 (2003) 999–1007, doi:10.1016/j.crci.2003.06.005.
[14] L. Pinto, B. Goi, C. Schmitt, M. Neumann, Photodegradation of polystyrene films containing UV-visible sensitizers, J. Res. Updat. Polym. Sci. 2 (2013).
[15] K. Woan, G. Pyrgiotakis, W. Sigmund, Photocatalytic Carbon-Nanotube–TiO2 Composites, Adv. Mater. 21 (2009) 2233–2239, doi:10.1002/adma.200802738.
[16] H. Zhu, S. Yan, Z. Li, Z. Zou, Back Electron Transfer at TiO2 Nanotube Photoanodes in the Presence of a H2O2 Hole Scavenger, ACS Appl. Mater. Interfaces. 9 (2017) 33887–33895, doi:10.1021/acsami.7b09827.
[17] D.R. Dreyer, S. Park, C.W. Bielawski, R.S. Ruoff, The chemistry of graphene oxide, Chem. Soc. Rev. 39 (2010) 228–240, doi:10.1039/B917103G.
[18] K.S. Novoselov, A.K. Geim, S.V Morozov, D. Jiang, Y. Zhang, S.V Dubonos, I.V Grigorieva, A.A. Firsov, Electric Field Effect in Atomically Thin Carbon Films, Science (80-.) 306 (2004) 666–669, doi:10.1126/science.1102896.
[19] C. Lee, X. Wei, J.W. Kysar, J. Hone, Measurement of the elastic properties and intrinsic strength of monolayer graphene, Science (80-.) 321 (2008) 385–388.
[20] A.A. Balandin, S. Ghosh, W. Bao, I. Calizo, D. Teweldebrhan, F. Miao, C.N. Lau, Superior Thermal Conductivity of Single-Layer Graphene, Nano Lett 8 (2008) 902–907, doi:10.1021/nl0731872.
[21] X. Huang, X. Qi, F. Boey, H. Zhang, Graphene-based composites, Chem. Soc. Rev. 41 (2012) 666–686, doi:10.1039/C1CS15078B.
[22] E. Singh, H.S. Nalwa, Stability of graphene-based heterojunction solar cells, RSC Adv 5 (2015) 73575–73600, doi:10.1039/C5RA11771B.
[23] U. Naknikham, V. Boffa, G. Magnacca, A. Qiao, L.R. Jensen, Y. Yue, Mutual-stabilization in chemically bonded graphene oxide–TiO2 heterostructures synthesized by a sol–gel approach, RSC Adv 7 (2017) 41217–41227, doi:10.1039/C7RA07472G.
[24] G. Williams, B. Seger, P.V Kamat, TiO2-Graphene Nanocomposites. UV-Assisted Photocatalytic Reduction of Graphene Oxide, ACS Nano 2 (2008) 1487–1491, doi:10.1021/nn800251f.
[25] W.S. Hummers, R.E. Offeman, Preparation of Graphitic Oxide, J. Am. Chem. Soc. 80 (1958) 1339, doi:10.1021/ja01539a017.
[26] T.V.M. Sreekanth, M.-J. Jung, I.-Y. Eom, Green synthesis of silver nanoparticles, decorated on graphene oxide nanosheets and their catalytic activity, Appl. Surf. Sci. 361 (2016) 102–106, doi:10.1016/j.apsusc.2015.11.146.
[27] D.C. Marcano, D.V Kosynkin, J.M. Berlin, A. Sinitskii, Z. Sun, A. Slesarev, L.B. Alemany, W. Lu, J.M. Tour, Improved Synthesis of Graphene Oxide, ACS Nano 4 (2010) 4806–4814, doi:10.1021/nn1006368.
[28] A.M. Dimiev, J.M. Tour, Mechanism of Graphene Oxide Formation, ACS Nano 8 (2014) 3060–3068, doi:10.1021/nn500606a.
[29] S. Lowe, Y.L. Zhong, Challenges of Industrial-Scale Graphene Oxide Production: Fundamentals and Applications, Graphene Oxide Fundam. Appl. (2016) 410–431, doi:10.1002/9781119069447.ch13.
[30] D. Chen, L. Zou, S. Li, F. Zheng, Nanospherical like reduced graphene oxide decorated TiO2 nanoparticles: an advanced catalyst for the hydrogen evolution reaction, Sci. Rep. 6 (2016) 20335, doi:10.1038/srep20335.
[31] Q. Xiang, J. Yu, M. Jaroniec, Graphene-based semiconductor photocatalysts, Chem. Soc. Rev. 41 (2012) 782–796.
[32] P. Gao, A. Li, D.D. Sun, W.J. Ng, Effects of various TiO2 nanostructures and graphene oxide on photocatalytic activity of TiO2, J. Hazard. Mater. 279 (2014) 96–104, doi:10.1016/j.jhazmat.2014.06.061.
[33] M. Khannam, S. Sharma, S. Dolui, S.K. Dolui, A graphene oxide incorporated TiO2 photoanode for high efficiency quasi solid state dye sensitized solar cells based on a poly-vinyl alcohol gel electrolyte, RSC Adv 6 (2016) 55406–55414, doi:10.1039/C6RA07577K.
[34] X. Rong, F. Qiu, C. Zhang, L. Fu, Y. Wang, D. Yang, Preparation, characterization and photocatalytic application of TiO 2 – graphene photocatalyst under visible light irradiation, Ceram. Int. (2014) 1–10, doi:10.1016/j.ceramint.2014.10.072.
[35] S.D. Perera, R.G. Mariano, K. Vu, N. Nour, O. Seitz, Y. Chabal, K.J. Balkus, Hydrothermal Synthesis of Graphene-TiO2 Nanotube Composites with Enhanced Photocatalytic Activity, ACS Catal 2 (2012) 949–956, doi:10.1021/cs200621c.
[36] H. Arami, M. Mazloumi, R. Khalifehzadeh, S.K. Sadrnezhaad, Sonochemical preparation of TiO2 nanoparticles, Mater. Lett. 61 (2007) 4559–4561, doi:10.1016/j.matlet.2007.02.051.
[37] H. Zhang, L.-H. Guo, D. Wang, L. Zhao, B. Wan, Light-Induced Efficient Molecular Oxygen Activation on a Cu(II)-Grafted TiO2/Graphene Photocatalyst for Phenol Degradation, ACS Appl. Mater. Interfaces. 7 (2015) 1816–1823, doi:10.1021/am507483q.
[38] Y. Zhang, Z.-R. Tang, X. Fu, Y.-J. Xu, Engineering the Unique 2D Mat of Graphene to Achieve Graphene-TiO2 Nanocomposite for Photocatalytic Selective Transformation: What Advantage does Graphene Have over Its Forebear Carbon Nanotube? ACS Nano 5 (2011) 7426–7435, doi:10.1021/nn202519j.
[39] S. Umrao, S. Abraham, F. Theil, S. Pandey, V. Ciobota, P.K. Shukla, C.J. Rupp, S. Chakraborty, R. Ahuja, J. Popp, B. Dietzek, A. Srivastava, A possible mechanism for the emergence of an additional band gap due to a Ti–O–C bond in the TiO2–graphene hybrid system for enhanced photodegradation of methylene blue under visible light, RSC Adv 4 (2014) 59890–59901, doi:10.1039/C4RA10572A.
[40] R.A. Rakkesh, D. Durgalakshmi, S. Balakumar, Efficient sunlight-driven photocatalytic activity of chemically bonded GNS–TiO2 and GNS–ZnO heterostructures, J. Mater. Chem. C. 2 (2014) 6827–6834, doi:10.1039/C4TC01195C.
[41] Q. Huang, S. Tian, D. Zeng, X. Wang, W. Song, Y. Li, W. Xiao, C. Xie, Enhanced Photocatalytic Activity of Chemically Bonded TiO2/Graphene Composites Based on the Effective Interfacial Charge Transfer through the C–Ti Bond, ACS Catal 3 (2013) 1477–1485, doi:10.1021/cs400080w.
[42] V. Štengl, S. Bakardjieva, T.M. Grygar, J. Bludská, M. Kormunda, TiO 2-graphene oxide nanocomposite as advanced photocatalytic materials, Chem. Cent. J. 7 (2013) 41.

[43] R. López, R. Gómez, Band-gap energy estimation from diffuse reflectance measurements on sol-gel and commercial TiO2: a comparative study, J. Sol-Gel Sci. Technol. 61 (2012) 1–7, doi:10.1007/s10971-011-2582-9.
[44] Z. Jiang, K. Qian, C. Zhu, H. Sun, W. Wan, J. Xie, H. Li, P.K. Wong, S. Yuan, Carbon nitride coupled with CdS-TiO2 nanodots as 2D/0D ternary composite with enhanced photocatalytic H2 evolution: A novel efficient three-level electron transfer process, Appl. Catal. B Environ. 210 (2017) 194–204, doi:10.1016/j.apcatb.2017.03.069.
[45] K. Alamelu, V. Raja, L. Shiamala, B.M. Jaffar Ali, Biphasic TiO2 nanoparticles decorated graphene nanosheets for visible light driven photocatalytic degradation of organic dyes, Appl. Surf. Sci. 430 (2018) 145–154, doi:10.1016/j.apsusc.2017.05.054.
[46] D. lal S, S.J. T, R. C, Solid-phase photodegradation of polystyrene by nano TiO2 under ultraviolet radiation, Environ. Nanotechnology, Monit. Manag. 12 (2019) 100229, doi:10.1016/j.enmm.2019.100229.